Soft Matter

Cite this: *Soft Matter*, 2011, **7**, 3108

www.rsc.org/softmatter

PAPER

Microtubule nanospool formation by active self-assembly is not initiated by thermal activation†

Isaac Luria,‡[a] Jasmine Crenshaw,‡[a] Matthew Downs,‡[ab] Ashutosh Agarwal,[ab] Shruti Banavara Seshadri,[a] John Gonzales,[b] Ofer Idan,[b] Jovan Kamcev,[b] Parag Katira,[a] Shivendra Pandey,[a] Takahiro Nitta,[c] Simon R. Phillpot[a] and Henry Hess*[b]

Received 10th August 2010, Accepted 18th November 2010
DOI: 10.1039/c0sm00802h

Biotinylated microtubules partially coated with streptavidin and gliding on a surface coated with kinesin motors can cross-link with each other and assemble into nanospools with a diameter of a few micrometres. The size distribution of these nanospools is determined, and it is shown with simulations of microtubule gliding that these spools are too small to be formed by thermally activated turns in the gliding direction (a Brownian ratchet mechanism). Instead, spool formation is primarily the result of two processes: pinning of gliding microtubules to inactive motors and simultaneous cross-linking of multiple microtubules.

Introduction

"How far can we push chemical self-assembly?" is one of the big questions in science.[1] One approach to overcome the limitations in component size, assembly speed and structural characteristics of chemical self-assembly is to utilize active transport rather than diffusion as the mechanism to achieve the recruitment and assembly of building blocks into a larger structure.[2] Active transport, for example driven by molecular motors, can move larger components faster than diffusion. Also, the spectrum of forces exerted during and after assembly by active transport is dramatically different from the spectrum of thermal forces present during and after equilibrium self-assembly. As a result, the assembly of non-equilibrium structures, such as structures under high internal strain, should be possible.

A simple model system for active self-assembly is the assembly of "sticky" microtubules gliding on a surface coated with kinesin motor proteins into "nanospools".[3,4] Biotinylated microtubules form when thousands of biotinylated tubulin proteins polymerize into tubular filaments with a diameter of 25 nm and a length of several micrometres, and they can bind to kinesin motor proteins adhered to a surface.[5] When these microtubules are partially coated with streptavidin, they become "sticky" because biotin–streptavidin–biotin cross-links can form. When gliding sticky microtubules collide, they assemble into elongated bundles. When the tip of a bundle encounters the middle of the bundle after a sharp turn, a "spool" begins to form (Fig. 1).

These spools typically have diameters of a few micrometres, which means that their formation from bundles of microtubules, each having a persistence length on the order of millimetres,[6–8] consumes a significant amount of energy. This energy amount on the order of thousands of kT has to be supplied by the hydrolysis of ATP and transduced by the motors. Spool formation is thus an "active", energy-consuming self-assembly process, but it has to be distinguished from "dynamic self-assembly",[9] since the spool is stable even when the energy flow ceases.

The first question of interest here is if the initiation of spool formation is the result of thermal fluctuations or the result of motor action. The answer is of considerable interest, because—compared to a process purely controlled by the motor action—an active self-assembly process which utilizes a thermally activated process as a rate-limiting step is significantly less amenable to engineering control. The second question we seek to answer is: what controls the size of the spool formed?

To answer these questions, we measure the size distribution of microtubule nanospools, and show, using computer simulations of gliding bundles, that thermal fluctuations in gliding directions result in spools which are four times larger in diameter than the experimentally observed spools. We then discuss the outcome of three alternative mechanisms of spool initiation: temporary pinning of the tip of the gliding microtubule bundle at defective motors, simultaneous cross-linking of multiple microtubules into a ring structure, and tip binding of motors.

In a recent publication,[4] Liu *et al.* proposed that spool formation results from bending of the tip of a microtubule or a microtubule bundle as a second microtubule wraps around it

[a]*Department of Materials Science and Engineering, University of Florida, Gainesville, FL, 32611-6400, USA*
[b]*Department of Biomedical Engineering, Columbia University, New York, NY, 10027-8904, USA. E-mail: hh2374@columbia.edu; Fax: +1 212-854-8725; Tel: +1 212-854-7749*
[c]*Department of Mathematical and Design Engineering, Gifu University, Gifu, 501-1193, Japan*

† Electronic supplementary information (ESI) available: The derivation of eqn (7). See DOI: 10.1039/c0sm00802h

‡ The marked authors contributed equally to this work.

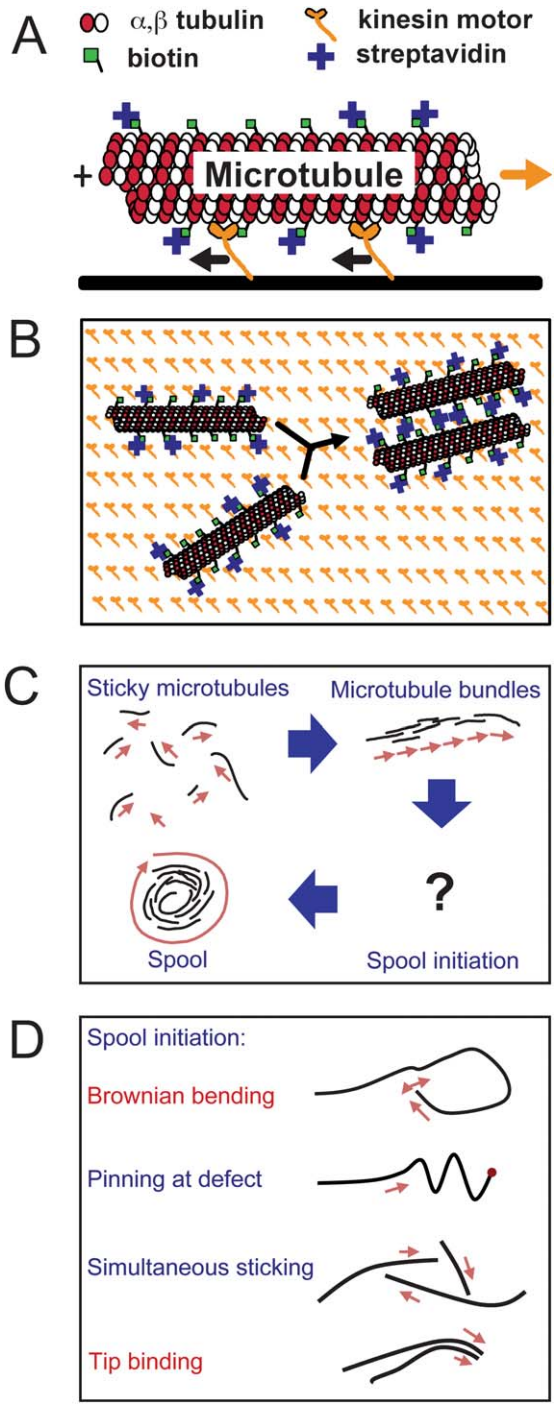

Fig. 1 (A) Microtubules are polymerized from α,β tubulin dimers functionalized with biotin linkers. Partial coverage of these linkers with tetravalent streptavidin enables cross-linking of microtubules. (B) Kinesin motor proteins adsorbed to the surface transport these "sticky" microtubules using ATP as a source of chemical energy. (C) Collisions between sticky microtubules lead to the formation of elongated bundles and finally spools. (D) Initiation of spool formation from microtubule bundles can potentially result from thermally activated fluctuations in the direction of the microtubule movement (Brownian bending), pinning at defective kinesin motors, simultaneous aggregation into a ring-like structure, or tip-binding of microtubules moving at different velocities. (A) and (B) reproduced with permission from ref. 3 Copyright 2005 American Chemical Society.

(due to the rotary motion of some microtubules[10]). We have re-enacted this process with a variety of macroscopic tubular structures and were unable to find any bending induced by the wrapping motion. Therefore we do not include this mechanism in our discussion.

The newly developed understanding of the spool formation process can be utilized to optimize the active self-assembly process, for example in order to favor the production of long bundles over spools.

Experimental results

After biotin/streptavidin-covered microtubules adhere in random orientations to the kinesin-coated surface, they are transported by the kinesin motors at a velocity of 0.6–0.8 μm s^{-1}, and collide with and bind to each other forming extended linear bundles. These "nanowires" continue to glide on the surface and within 20 min have mostly morphed into circular aggregates ("nanospools", Fig. 2A). Several hundreds of these spools are imaged (in different fields of view and different experiments).

While the imaging of the spools is typically conducted only after the formation of the spools has been completed in order to avoid interference of the fluorescence excitation light with the assembly process, times-lapse images are collected in some experiments.

From these time-lapse data, it is apparent that the spool formation is often initiated by the pinning of the microtubule tip to the surface (Fig. 2B and C). These pinning events are well-known[11] and typically attributed to a defective motor which is able to bind but not transport a microtubule. In a previous study they occurred on average once every 750 μm along the path of a microtubule.[12] However, caution is required when generalizing these observations for two reasons. Firstly, exposure to the intense fluorescence excitation light can cause cross-linking of microtubules to kinesin, potentially causing increased pinning during observation.[13,14] Secondly, imaging commences at the earliest a minute after microtubule movement has begun, and during that time many microtubule bundles and some spools have already formed.

A second formation mechanism (Fig. 2D) was observed only after being discovered in simulations of the assembly process (simulations described below). Three (or more) microtubules approaching each other simultaneously can cross-link in a triangular shape, which then relaxes into a circular shape over time. This process is favored in the first few seconds of the assembly process, when microtubule surface densities are highest.

The length distribution of microtubules and microtubule bundles is determined by manually measuring the length of the structures observed in several experiments using image analysis software. The length distribution peaks at a length of 6 μm and then decays rapidly (Fig. 3A). It can be fit with a distribution $p(L) = B \times L \times e^{-AL} + C \times (L/D) \times e^{-AL/D}$ with parameters $A =$ 0.22 μm^{-1}, $B = 4.8$ μm^{-1}, $C = 0.93$ μm^{-1} and $D = 4.4$. The first term of this distribution represents the Schulz distribution of microtubule lengths and approximates the initial length distribution of microtubules.[15] The second term approximates the contribution of microtubule bundles, which are on average about four times longer than the individual microtubules.

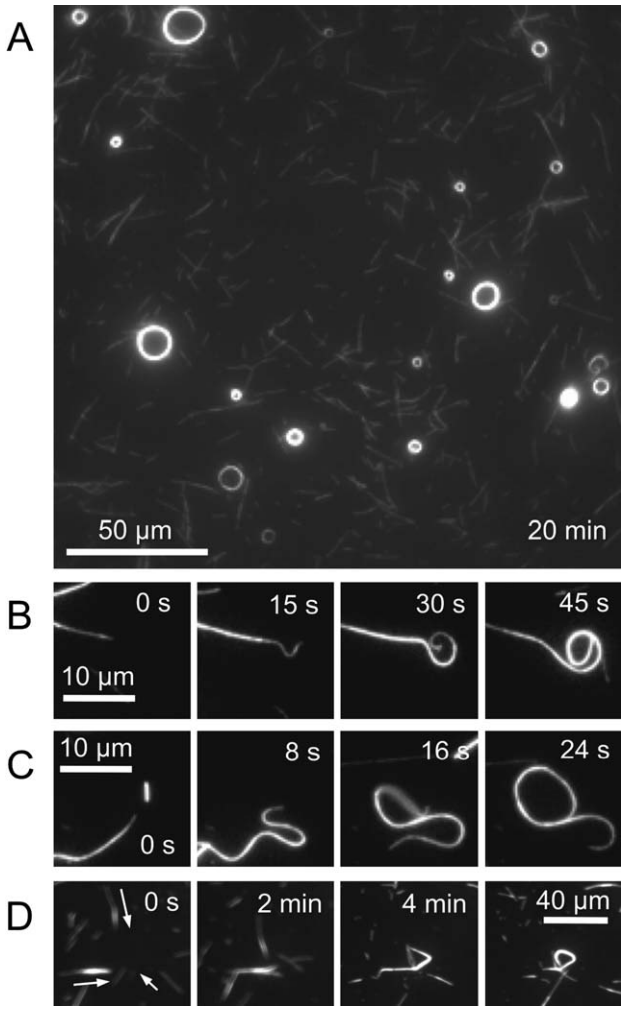

Fig. 2 (A) Aggregation of microtubules leads to the formation of spools of different sizes. (B and C) Pinning of the leading tip of a microtubule bundle initiates spool formation. (D) Simultaneous collisions of three (or more) microtubule bundles form triangular structures relaxing into circular spools.

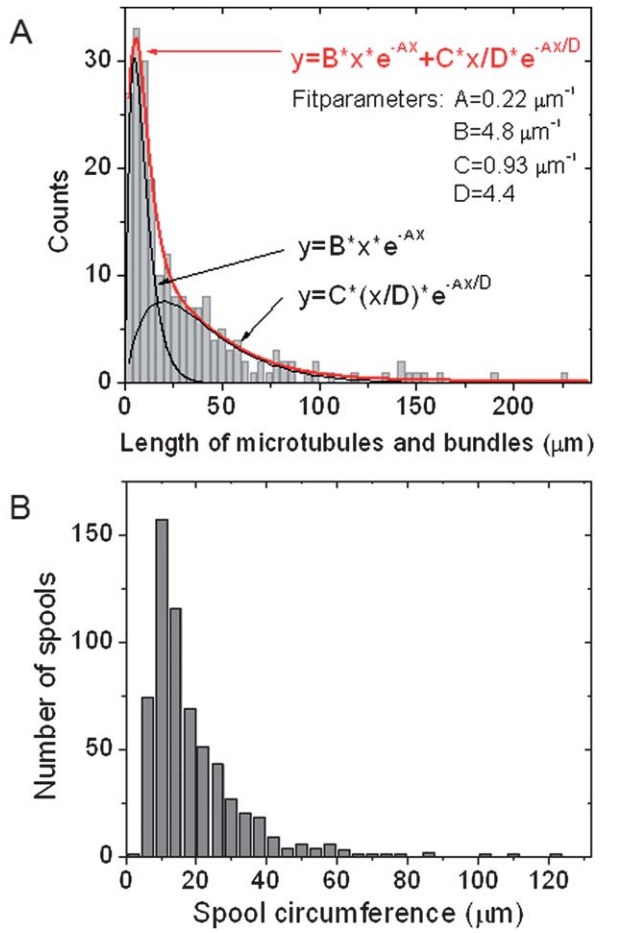

Fig. 3 (A) Experimental length distribution of microtubules and microtubule bundles after 20 min aggregated from 3 separate experiments. (B) Experimental size distribution of spools. A total of 607 spools were measured.

The size distribution of the spools which have formed after at least 20 min peaks at a circumference of about 10 μm, and exponentially decays towards larger sizes (Fig. 3B). Spools with circumferences smaller than 6 μm are not observed. The circumference is used as a metric here, since some of the larger spools are asymmetric, making the determination of a diameter more ambiguous. To obtain a sufficient number of spools for a statistical analysis, we have pooled the data from four separate experiments with streptavidin concentrations during assembly of 5–20 nM. The spool images of the four experiments were qualitatively the same.

Simulations and analytical results

Spool formation resulting from thermally activated bending

The spool assembly process is first simulated using the method by Nitta *et al.*, which models the thermal fluctuations of the microtubule tip and the ensuing microtubule trajectory with the characteristics of a worm-like chain.[16] In an off-lattice Monte Carlo simulation, trajectories of gliding microtubules are generated by advancing microtubules in discrete time steps of 100 ms. The direction and length of the microtubule gliding steps are varied to reproduce the previously determined persistence length of the trajectory (0.1 mm) and the motional diffusion coefficient of the gliding motion (0.002 $\mu m^2\ s^{-1}$).[12] The motional diffusion coefficient measures the diffusive component of the gliding motion, which is superimposed on the smooth gliding of the microtubule.

A single trajectory of 45 mm is generated and used to represent the approximately 100 microtubules gliding with a velocity of 450 nm s^{-1} for ~1000 s during the assembly process within a field of view. The entire trajectory is examined for "loops", which are defined as segments where the trajectory intersects with itself for the first time since the last intersection (Fig. 4A). To determine the length of the loop segment, a length counter is started at the beginning of the simulation, each newly generated segment is checked for intersections with segments generated since the start of the loop counter, and if an intersection is found, the length of the formed loop is stored and the length counter is reset.

The frequency count of loop circumferences peaks at roughly 500 μm (Fig. 4B). However, only trajectory loops with a circumference smaller than the length of the microtubule

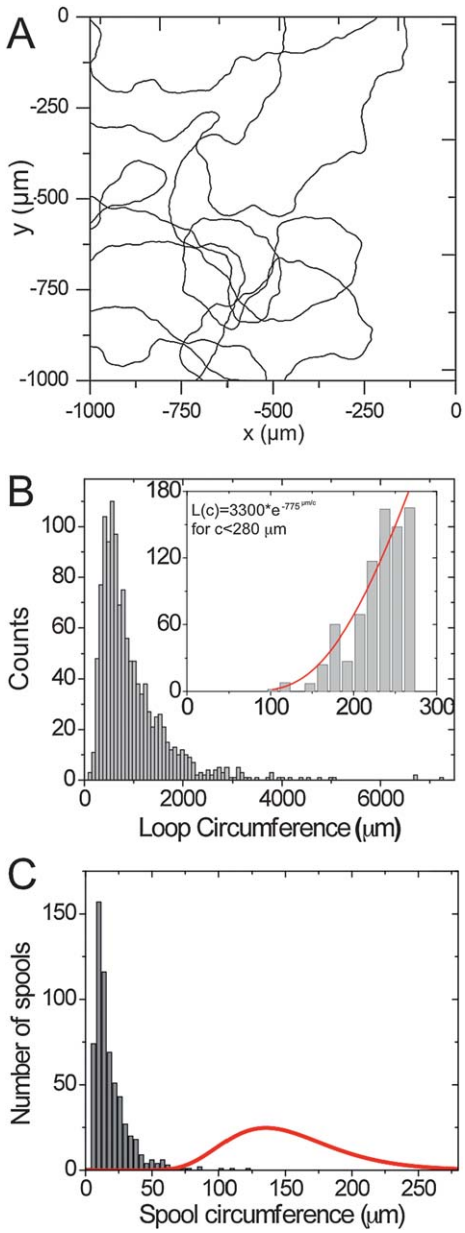

Fig. 4 A simulated trajectory (A) is utilized to determine the distribution of loop circumferences (B). The inset shows the frequency of small circumferences and the fit to this distribution. Loops can result in spool formation if the microtubule bundle is of sufficient length. With the knowledge of the microtubule length distribution (Fig. 3) and the loop circumference distribution, the expected size distribution of spools formed by thermal fluctuations can be calculated (C, red curve) and compared to the experimental size distribution of spools (C, grey bars).

bundle tracing it can result in a collision between the tip and the center (or tail) of the microtubule bundle and the initiation of spool formation. Thus, the circumference distribution of spool initiation events is given by:

$$S(c) = L(c)\int_{c}^{\infty} M(l)dl \qquad (1)$$

where $S(c)$ is the distribution of initiated spool circumferences, $M(l)$ is the length distribution of microtubules and bundles (Fig. 3A), and $L(c)$ is the simulated distribution of loop circumferences (Fig. 4A).

A technical difficulty is that since microtubules and microtubule bundles have primary lengths of less than 200 μm, it is critical to determine the loop distribution function for circumferences of less than 200 μm with high accuracy. We obtained a more detailed histogram of such short loops (inset Fig. 4B) by extending the length of the simulated trajectory a hundred-fold and only recording the occurrence of short loops for computational efficiency. The histogram is then fit with a function of the type $L(c) = L_0 \times e^{c_0/c}$, since a Boltzmann distribution of the bending energy for each loop ($E_B \approx 1/c$) is expected. A good fit is obtained for the parameters $L_0 = 3307$ and $c_0 = 775$ μm.

If we assume that such a spool initiation results in an actual spool formation with a probability independent of the loop circumference, the resulting distribution $S(c)$ is also the simulated spool diameter distribution (Fig. 4C). The distribution of spool circumferences based on the thermally activated directional changes in gliding direction ("Brownian bending") has a roughly Gaussian shape peaking at 130 μm.

Spool formation resulting from pinning events

Close observation of the spool formation process shows that spools can form following a microtubule tip pinning event. As the leading tip of a microtubule or a microtubule bundle gliding on a kinesin coated surface gets stuck to a defective (non-functional) kinesin, the force from the other kinesins attached to the microtubule buckles the microtubule.[11,17]

The specific sequence of events leading to the formation of a spool after pinning can be varied and is complex (Fig. 2).[3] However, successful formation of a spool with a given circumference c requires: (1) a sufficiently long microtubule or microtubule bundle and (2) a sufficiently large number of attachment points between microtubules and motors to support the bending stress on the microtubule.

The probability that both conditions are fulfilled is the product of the individual probabilities and depends on the circumference of the forming spool among other parameters:

$$P(C) = P_{\text{length}}(C) \times P_{\text{motor}}(C) \qquad (2)$$

The probability P_{length} that a randomly chosen microtubule or microtubule bundle is at least of length C is given by the complement of the cumulative length distribution. The length distribution evolves during the spool assembly process from the initial length distribution of individual microtubules to a length distribution with an increasing fraction of microtubule bundles (Fig. 3) as microtubules collide and assemble.

The probability P_{motor} that a sufficient number of motors hold the forming spool increases with the spool circumference since the exerted bending moment decreases and the number of motors increases. For simplicity, we assume that there is a minimal spool radius below which motors always let go of the attached microtubule, while attachment is always sustained at larger radii (smaller forces). The rupture force for each kinesin microtubule bond is approximately 3 pN[18] and the bending force of a circular rod is given by $F = \pi EI/R^2$.[19] This minimal radius to which a buckling microtubule can be bent by the kinesins is given by:

$$R = \sqrt{\frac{\pi k_B T L_p}{nF}} \quad (3)$$

where k_B is the Boltzmann constant, T is the temperature, L_p is the persistence length of the microtubule, n is the number of kinesin motors attached to the buckled section of the microtubule and F is the binding force between a kinesin and the microtubule.

Since the kinesin motors are randomly distributed on the surface, the requirement that the minimum radius is exceeded translates into a requirement that for a given circumference at least a minimum number of motors are attached. This minimum number is:

$$n = \text{ceiling}\left(\frac{4\pi^3 k_B T L_p}{FC^2}\right) \quad (4)$$

Since the number of attached motors along a microtubule segment of length C is Poisson distributed around the mean $\langle n \rangle = \rho w C$ where $\rho = 150\ \mu m^{-2}$ and $w = 25$ nm,[20] the probability that at least n motors are attached is given by the complement of the cumulative distribution function:

$$P(k \geq n) = 1 - \Gamma(n, \langle n \rangle)/(n-1)! \quad (5)$$

where Γ is the incomplete γ-function. Combining eqn (2) and (5) yields:

$$P(C) = \left(1 - \frac{\int_0^C p(L)\mathrm{d}L}{\int_0^\infty p(L)\mathrm{d}L}\right)\left(1\frac{\Gamma(n, \rho w C)}{(n-1)!}\right) \quad (6)$$

with $p(L)$ as the microtubule length distribution fitted above (Fig. 3A).

The appropriate choice for the microtubule persistence length is an interesting question, since the microtubule is a complex mechanical structure whose stiffness depends on the experimental context.[6,21–23] Pampaloni *et al.* explained their observations of a length-dependent persistence length by the limited longitudinal displacement between adjacent protofilaments enabled by bending lateral bonds.[6] This limited displacement conveys high flexibility to a bending microtubule as long as the bending requires only small displacements between tubulins in adjacent protofilaments (applies to a large radius of curvature or a short microtubule). The microtubule stiffens when bending increases as the lateral bonds cannot accommodate the displacement by bending alone. In our case, we believe that the large bending of the microtubule during spool formation results in a stiff response with a large persistence length of 5 mm.[8] The persistence length of the microtubule also has to be distinguished from the smaller persistence length of the microtubule trajectory (0.1 mm) which results from small fluctuations of the microtubule tip only and is employed in the off-lattice simulations described above. Under these assumptions for L_p, F, ρ, and w, a minimal spool diameter of ~2 μm (circumference of ~6 μm) is obtained, in good agreement with previous observations.[11,17]

The experimentally determined histogram of spool circumferences is compared to the model predictions for two length distributions (Fig. 5): the initial length distribution of individual microtubules (as inferred from the contribution of microtubules to the fit in Fig. 3A) and the final length distribution of microtubules and microtubule bundles (fit in Fig. 3A). The model reproduces the frequent occurrence of spool circumferences beyond a minimal value well. The exponential decrease in frequency of larger spools is also reproduced. However, the experimental data fall between the two extreme scenarios for the microtubule length distribution, as one would reasonably expect.

Spool formation resulting from simultaneous sticking

A novel simulation code[24] enables the simulation of hundreds of microtubules gliding on a surface and interacting with each other. In the simulation, microtubules represented as segmented chains move on a triangular lattice with periodic boundary conditions and bind to each other at each collision (lattice size 2400 × 2400, segment size 80 nm, initially 1250 microtubules of 5 μm length, results averaged over 200 runs with 30 000 time steps).

Surprisingly, a random distribution of microtubules of average length and surface density similar to the microtubule population used in the experiment evolves into spools with a size distribution which is very close to the experimentally observed size distribution (Fig. 6), even if—unlike in the experiments—the microtubules are confined to movements on straight lines (unless they meet another microtubule and join it). However, spool formation is mostly complete within the first minute of simulated microtubule movement.

Since in these simulations microtubules cannot turn by themselves, and since pinning events are not part of the simulation, the formation of spools in these simulations is entirely the result of simultaneous collisions between multiple microtubules. The obtained size distribution makes intuitive sense: it is unlikely that three or more microtubules meet at their tips and create a tiny spool; it is highly likely that they meet somewhere in their middles and create a spool with a circumference of three times half the average microtubule length; it becomes increasingly unlikely that very long microtubules or microtubule bundles

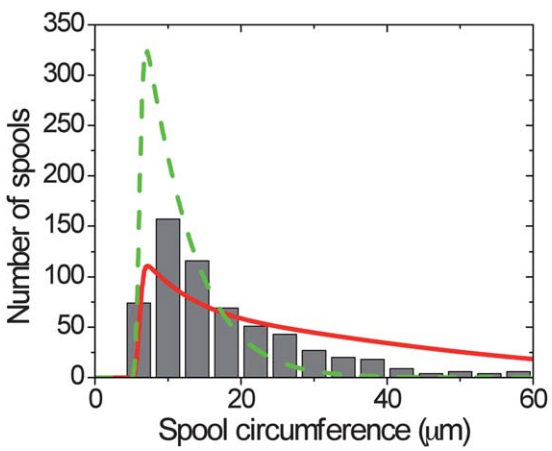

Fig. 5 Comparison between the analytical model predictions (green dashed curve: single microtubule length distribution; red solid curve: microtubule and microtubule bundle length distribution) and the experimentally observed distribution of spool circumferences from Fig. 3B (grey bars). Predicted circumference distributions are normalized to a total of 607 spools.

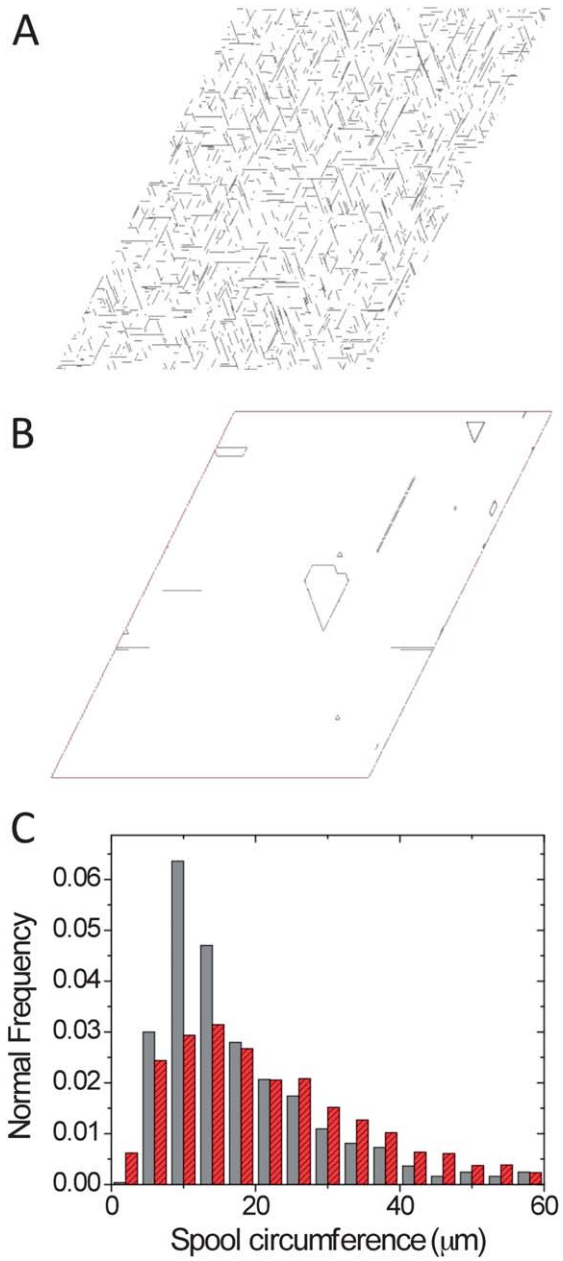

Fig. 6 Initial (A) and final (B) snapshots of a run of the lattice simulation of microtubule spool formation. (C) Comparison between the circumference distributions of spools formed in the lattice simulation (red hashed bars) and the experimentally observed distribution of spool circumferences from Fig. 3B (grey bars, normalized).

(which are rare) participate in the simultaneous collision to create large spools.

Spool formation resulting from tip collisions

Collisions of two microtubules or microtubule bundles at their very tips can potentially lead to a circular trajectory, which subsequently leads to spool formation, if the two microtubules move at different velocities (Fig. 1D—tip binding). Microtubule gliding velocities have been measured to vary 3% around the mean (standard deviation),[12] and these velocity differences have to be accommodated during cross-linking by acceleration and deceleration of the slower and faster microtubule. However, in situations where the tips meet, a fraction of the velocity difference can be accommodated by bending towards the slower microtubule. As cross-linking proceeds along the microtubule, this curvature is locked in the bundle structure and causes the bundle to follow a circular trajectory. If the bundle is sufficiently long, the circular trajectory causes the formation of a spool.

For clarification of this mechanism it should be pointed that almost all spools eventually relax to a circular shape, but they do not have to form from a circular trajectory. Pinning events as well as simultaneous sticking (see above) create spools but do not start with circular trajectories. The "tip" of a microtubule or a microtubule bundle is the segment of the leading end which fluctuates due to Brownian motion, and whose attachment to new motors forces the remaining microtubule to follow its path. The length of the "tip" is less than a micrometre, but several motors are attached to it.

Assuming that the microtubule velocities follow a Gaussian distribution with a variance σ^2 of approximately 10^{-3} μm^2 s^{-2},[12] the probability that the two interacting microtubule tips have a velocity difference which causes a circular trajectory with circumference C, $P_{\Delta v}(C)$, is given by (see ESI†):

$$P_{\Delta v}(C) = P_{\Delta v}(\Delta v = 2\pi v D/C) = \frac{4\pi D v}{C^2\sqrt{4\pi\sigma^2}} e^{-\left(\frac{\pi D v}{C\sigma}\right)^2} \quad (7)$$

where $D = 30$ nm is the center to center distance between the two microtubules, and $v = 0.8$ μm s^{-1} is the average gliding velocity. A back-of-the-envelope estimate shows the force required for tip bending is small and does not significantly slow the microtubules relative to each other. The above probability distribution peaks at a circumference of 2.5 μm, with 60% of the cumulative probability lying below the minimum spool circumference of ~6 μm (see Fig. 5).

This mechanism is therefore expected to create primarily spools of the smallest possible circumference. An associated peak in the spool size distribution is not observed experimentally, which seems unsurprising considering the low probability of two microtubules meeting exactly at their tips. However, on rare occasion a microtubule bundle following a circular trajectory has been observed, which suggests that the mechanism cannot be ruled out entirely.

Discussion and conclusions

The experimentally determined distribution of spool circumferences (Fig. 3) is in good agreement with previous observations,[3,4,25–28] even though the morphology of spools obtained by cross-linking with streptavidin is somewhat different from the morphology of spools obtained by cross-linking with streptavidin-functionalized quantum dots.[4,25] Specifically, the formation of broad spools with significantly different inner and outer diameters is less prominent here.

Our off-lattice simulations of the loop formation process (Fig. 1D—Brownian bending) reveal that the selection bias towards smaller loops due to the limited length of the microtubule bundles is capable of producing surprisingly small spools (circumferences of 100–200 μm) compared to the average size of

the loops in the trajectory. However, the experimentally observed spools are still smaller (circumference < 40 μm), so that spool formation due to thermal fluctuations in the gliding direction cannot account for the experimental observations. Furthermore, the off-lattice simulation is likely to overestimate the frequency of occurrence of small loops, because it does not consider the increasing microtubule stiffness due to prior bending suggested by Pampaloni *et al.*[6]

In contrast, the analytical modeling of a mechanism dependent on the mechanical work exerted by the motors, specifically the bending of the microtubule against the stationary tip pinned by a defective motor (Fig. 1D—pinning at defect), produces a picture in accord with the experimental observations. The absence of very small spools (<6 μm circumference) is explained as a result of the inability of the motors holding the bending microtubule to provide sufficient attachment force. The declining frequency of larger spools is due to the declining prevalence of sufficiently long microtubule bundles.

These considerations do not take into account the detailed mechanics of the 'spool formation by pinning' process. For example, we have observed microtubule tips which remain attached to the pinning motor during the entire spool formation process; an event which results in small spools. We have also observed release of microtubule tips from the pinning motor before a spool has fully formed, and only the subsequent collision of the bent front section with the center or tail section of the microtubule resulted in the formation of a larger spool. A more detailed modeling of the pinning process also has to account for the dynamic changes in the length distribution of microtubules and microtubule bundles within the first minute of the experiment. In combination, the increasing number of free parameters of such a model is not likely to lead to a proportional increase in our understanding.

The picture is complicated by the identification of the 'simultaneous sticking' route to spool formation (Fig. 1D—simultaneous sticking). Lattice simulations show that the cross-linking of three or more filaments into closed, ring-like structures which evolves into a circular spool can lead to a size distribution similar to the experimentally observed size distribution. The 'simultaneous sticking' process is expected to scale with the third power of the microtubule surface density, which makes it most likely to occur before significant bundling of microtubules took place. Unfortunately, these first few seconds of the assembly process are difficult to image with our current experimental setup.

The cross-linking of two microtubules at their tips (Fig. 1D—tip binding) can in principle give rise to a curved structure if the microtubule velocities are different, but spools of small diameters are expected to result from this process. No distinct peak is observed in the experimental data, and the small probability of such tip binding events makes it unlikely that this is a major contribution to spool formation.

The balance between 'spool formation by simultaneous sticking' and 'spool formation by pinning' is greatly affected by microtubule density. High density, implying frequent simultaneous collisions, favors the former, while low density, implying large distances between collisions and a high likelihood of encountering a defective motor, favors the latter. However, both processes lead to similar spool size distributions, which makes questions about the specific route less pressing.

The key insight is that spool formation is not activated by a Brownian ratchet type process, where rare and thermally activated bending events lead to spool formation. This result is important, because the fact that the formation of spools requires a significant amount of mechanical work to bend the microtubules is in itself not proof that it could not be accomplished by thermally activated self-assembly. The formation of biotin–streptavidin bonds releases free energy, which could conceivably cause a microtubule or microtubule bundle to step-by-step (or bond-by-bond) wrap around itself once a spool has been initiated by thermal fluctuations. Spool formation by thermal fluctuations can indeed lead to spools much smaller than the persistence length of the microtubules, as our simulations have shown, but not small enough to explain the experimental observations. Instead, our investigation has determined that the primary spool formation mechanisms are 'simultaneous collisions' and 'pinning'.

Our second goal was to identify a mechanism to control the spool size. Manipulation of the system parameters, such as initial microtubule density and length as well as kinesin density, can be expected to modify the spool size distribution. However, since spool size and size distribution seems to be very similar in different experiments under different conditions from different laboratories, the effects are likely to be small. This agrees with our analysis which shows that two very different formation mechanisms lead to very similar size distributions. The most productive approach to controlling spool size is likely to suppress 'spool formation by pinning' as well as 'spool formation by simultaneous sticking', and to guide the microtubule motion towards loops of defined sizes, for example in guiding channels.[29]

The broad technology trends towards miniaturized devices and complex materials create the need for advances in assembly methods beyond thermally activated self-assembly (also known as chemistry when the components are molecules) and robotics. Active self-assembly has the potential to make a contribution, and the kinesin/microtubule model system can be used to identify the principles underlying this approach.

Materials and methods

Full length, wild-type kinesin from *Drosophila melanogaster* expressed with a *C*-terminal histidine-tag in *Escherichia coli* was purified using a Ni-NTA column as described in ref. 30.

The employed antifade system consisted of 20 mM D-glucose, 20 mg ml^{-1} glucose oxidase, 8 mg ml^{-1} catalase, and 10 mM dithiothreitol.

Flow cells were assembled from glass slides, glass coverslips (Fisher's Finest, Fisher Scientific Inc.), and double sided tape and incubated with casein solution (0.5 mg ml^{-1} in BRB80 buffer: 80 mM PIPES, 1 mM $MgCl_2$, 1 mM ethylene glycol tetraacetic acid, pH 6.9) for 5 min. The casein solution was replaced with a kinesin solution (~10 nM kinesin, 1 mM ATP) for another 5 min.

One of two methods was used to assemble spools.

The first method used biotinylated microtubules (4 mg ml^{-1} biotinylated tubulin from Cytoskeleton Inc. polymerized for 30 min with 4 mM $MgCl_2$, 1 mM GTP, 5% dimethyl sulfoxide in BRB80 buffer and stabilized with 10 μM taxol) and fluorescently labeled streptavidin. The kinesin solution was replaced by microtubule solution (80 μg ml^{-1} microtubules, 0.5 mM ATP,

antifade system in BRB80) for 5 min. The microtubule solution was washed out twice with antifade solution (10 μM taxol, 0.5 mM ATP, 0.2 mg ml^{-1} casein, antifade system in BRB80). Streptavidin solution (20 nM Alexa-488 streptavidin from Molecular Probes Inc., 0.2 mg ml^{-1} casein, 10 μM taxol in BRB80) was injected for 5 min, and washed out twice with antifade solution.

The second method used biotinylated (90%) and rhodamine-labeled (10%) microtubules (3.6 mg ml^{-1} biotinylated tubulin and 0.4 mg ml^{-1} rhodamine-labeled tubulin from Cytoskeleton Inc. polymerized for 30 min with 4 mM $MgCl_2$, 1 mM GTP, 5% dimethyl sulfoxide in BRB80 buffer and stabilized with 10 μM taxol) and unlabeled streptavidin. The kinesin solution was replaced by microtubule solution (40 μg ml^{-1} microtubules, 1 mM ATP, antifade system in BRB80). After 5 min, the streptavidin solution (5, 8 or 12 nM unlabeled streptavidin from Sigma Inc. in BRB80 with antifade system) was injected. After another 5 min, the flow cell was washed thrice with antifade solution (10 μM taxol, 1 mM ATP, 0.2 mg ml^{-1} casein, antifade system in BRB80).

The flow cell was imaged on an epi-fluorescence microscope (Nikon TE2000) using a 100× oil objective (N.A. 1.4) and an iXON EMCCD camera (Andor Inc.).

Acknowledgements

Financial support through NSF grant DMR0645023 and helpful discussions with Marion Paolini are gratefully acknowledged.

References

1 R. F. Service, *Science*, 2005, **309**, 95.
2 H. Hess, *Soft Matter*, 2006, **2**, 669–677.
3 H. Hess, J. Clemmens, C. Brunner, R. Doot, S. Luna, K.-H. Ernst and V. Vogel, *Nano Lett.*, 2005, **5**, 629–633.
4 H. Q. Liu, E. D. Spoerke, M. Bachand, S. J. Koch, B. C. Bunker and G. D. Bachand, *Adv. Mater.*, 2008, **20**, 4476–4481.
5 J. Howard, *Mechanics of Motor Proteins and the Cytoskeleton*, Sinauer, Sunderland, MA, 2001.
6 F. Pampaloni, G. Lattanzi, A. Jonas, T. Surrey, E. Frey and E.-L. Florin, *Proc. Natl. Acad. Sci. U. S. A.*, 2006, **103**, 10248–10253.
7 M. E. Janson and M. Dogterom, *Biophys. J.*, 2004, **87**, 2723–2736.
8 F. Gittes, B. Mickey, J. Nettleton and J. Howard, *J. Cell Biol.*, 1993, **120**, 923–934.
9 G. M. Whitesides and B. Grzybowski, *Science*, 2002, **295**, 2418–2421.
10 B. Nitzsche, F. Ruhnow and S. Diez, *Nat. Nanotechnol.*, 2008, **3**, 552–556.
11 D. G. Weiss, G. M. Langford, D. Seitz-Tutter and W. Maile, *Acta Histochem., Suppl.*, 1991, **41**, 81–105.
12 T. Nitta and H. Hess, *Nano Lett.*, 2005, **5**, 1337–1342.
13 T. Surrey, M. B. Elowitz, P. E. Wolf, F. Yang, F. Nedelec, K. Shokat and S. Leibler, *Proc. Natl. Acad. Sci. U. S. A.*, 1998, **95**, 4293–4298.
14 P. Yan, Y. J. Xiong, B. W. Chen, S. Negash, T. C. Squier and M. U. Mayer, *Biochemistry*, 2006, **45**, 4736–4748.
15 Y. Jeune-Smith and H. Hess, *Soft Matter*, 2010, **6**, 1778–1784.
16 T. Nitta, A. Tanahashi, M. Hirano and H. Hess, *Lab Chip*, 2006, **6**, 881–885.
17 L. Bourdieu, T. Duke, M. B. Elowitz, D. A. Winkelmann, S. Leibler and A. Libchaber, *Phys. Rev. Lett.*, 1995, **75**, 176–179.
18 M. J. Schnitzer, K. Visscher and S. M. Block, *Nat. Cell Biol.*, 2000, **2**, 718–723.
19 H. Hess, J. Clemmens, C. M. Matzke, G. D. Bachand, B. C. Bunker and V. Vogel, *Appl. Phys. A: Mater. Sci. Process.*, 2002, **75**, 309–313.
20 P. Katira, A. Agarwal, T. Fischer, H.-Y. Chen, X. Jiang, J. Lahann and H. Hess, *Adv. Mater.*, 2007, **19**, 3171–3176.
21 M. G. L. van den Heuvel, S. Bolhuis and C. Dekker, *Nano Lett.*, 2007, **7**, 3138–3144.
22 P. J. Keller, F. Pampaloni, G. Lattanzi and E. H. K. Stelzer, *Biophys. J.*, 2008, **95**, 1474–1486.
23 Y. W. Gao and F. M. Lei, *Biochem. Biophys. Res. Commun.*, 2009, **387**, 467–471.
24 J. Crenshaw, T. Liang, H. Hess and S. R. Phillpot, *J. Comput. Theor. Nanosci.*, 2010, submitted.
25 M. Bachand, A. M. Trent, B. C. Bunker and G. D. Bachand, *J. Nanosci. Nanotechnol.*, 2005, **5**, 718–722.
26 R. Kawamura, A. Kakugo, Y. Osada and J. P. Gong, *Nanotechnology*, 2010, **21**, 145603.
27 R. Kawamura, A. Kakugo, Y. Osada and J. P. Gong, *Langmuir*, 2010, **26**, 533–537.
28 R. Kawamura, A. Kakugo, K. Shikinaka, Y. Osada and J. P. Gong, *Biomacromolecules*, 2008, **9**, 2277–2282.
29 J. Clemmens, H. Hess, R. Doot, C. M. Matzke, G. D. Bachand and V. Vogel, *Lab Chip*, 2004, **4**, 83–86.
30 D. L. Coy, M. Wagenbach and J. Howard, *J. Biol. Chem.*, 1999, **274**, 3667–3671.